Time-Resolved Fluorescence Anisotropy Study of the Refolding Reaction of the α-Subunit of Tryptophan Synthase Reveals Nonmonotonic Behavior of the Rotational Correlation Time†

Osman Bilsel,‡ Li Yang,§,|| Jill A. Zitzewitz,‡ Joseph M. Beechem,*,§ and C. Robert Matthews*,‡

Department of Chemistry and Center for Biomolecular Structure and Function, The Pennsylvania State University, University Park, Pennsylvania 16802, and Department of Molecular Physiology and Biophysics, Vanderbilt University, Nashville, Tennessee 37232

Received December 15, 1998; Revised Manuscript Received January 27, 1999

ABSTRACT: Time-resolved fluorescence anisotropy of a bound extrinsic probe was studied in an effort to characterize dynamic properties of the transient partially folded forms that appear during the folding of the α-subunit of tryptophan synthase (αTS) from *Escherichia coli.* Previous studies have shown that αTS, a single structural domain, can be cleaved into autonomously folding amino- and carboxy-folding units comprising residues 1−188 and 189−268, respectively [Higgins, W., Fairwell, T., and Miles, E. W. (1979) *Biochemistry 18,* 4827−4835]. By use of a double-kinetic approach [Jones, B. E., Beechem, J. M., and Matthews, C. R. (1995) *Biochemistry 34*, 1867−1877], the rotational correlation time of 1-anilino-8-naphthalene sulfonate bound to nonpolar surfaces of folding intermediates was measured by time-correlated single photon counting at varying time delays following initiation of folding from the urea-denatured form by stopped-flow techniques. Comparison of the rotational correlation times for the full-length αTS and the amino-terminal fragment suggests that folding of the amino-terminal fragment and carboxy-terminal fragment is coordinated, not autonomous, on the milliseconds to seconds time scale. If a spherical shape is assumed, the apparent hydrodynamic radius of αTS after 5 ms is 26.8 Å. The radius increases to 28.5 Å by 1 s before decreasing to the radius for native αTS, 24.7 Å, on a longer time scale (>25 s). Viewed within the context of the kinetic folding model of αTS [Bilsel, O., Zitzewitz, J. A., Bowers, K. E., and Matthews, C. R. (1999) *Biochemistry 38*, 1018−1029], the initial collapse reflects the formation of an off-pathway burst-phase intermediate in which at least part of the carboxy folding unit interacts with the amino folding unit. The subsequent increase in rotational correlation time corresponds to the formation of an on-pathway intermediate that leads to the native conformation. The apparent increase in the radius for the on-pathway intermediate may reflect a change in the interaction of the two-folding units, thereby forming a direct precursor for the α/β barrel structure.

Transient partially folded forms that appear during the folding of globular proteins are thought to provide insights into the process by which the conformational search space is narrowed in the acquisition of the native structure (*1*, *2*). One goal of characterizing these intermediates is to obtain a description of a complete reaction coordinate for protein folding. To this end, a variety of techniques have been interfaced to rapid-mixing systems to monitor formation of individual backbone hydrogen bonds (*3*−*7*), secondary structure content (*8*, *9*), point-to-point distances (*10*, *11*), and size (*12*−*14*), among other properties. The size and shape of folding intermediates are of particular interest because these parameters are more readily addressed by theoretical models and simulations of protein folding (*15*) than are specific molecular details. However, due to the low sensitivity of the small-angle X-ray scattering and light scattering techniques that have been used to measure the size of kinetic intermediates, relatively few measurements have been reported (*13*, *14*, *16*−*18*).

Time-resolved fluorescence anisotropy has been used for a number of years to probe the rotational dynamics of globular proteins via side-chain and ligand chromophores (*19*). When the probe chromophore is rigidly bound to the protein, the time-resolved anisotropy decay time constant can be considered proportional to the hydrated volume of the protein (*19*). The cubic dependence of the rotational correlation time on the hydrodynamic radius offers a potentially sensitive probe of size. Recently, Beechem and co-workers have merged this technique with stopped-flow technology commonly used in the study of protein folding reactions (*20*, *21*). The disparate time scales of fluorescence (nanoseconds) and typical stopped-flow protein folding reactions (>milliseconds) allows multiple time-correlated single-photon counting experiments to be completed during a single folding

† This work was supported by the National Institutes of Health through Grant GM23303 to C.R.M. and grants GM45990 and RR5823 to J.M.B. Additional support was obtained from The Lucille P. Markey Charitable Trust (J.M.B.). Partial support was also provided by NIH Postdoctoral Fellowship Awards GM17814 to O.B. and GM14954 to J.A.Z.

* To whom correspondence should be addressed. C.R.M.: e-mail crm@psu.edu; phone 814-865-8859; fax 814-863-8403. J.M.B.: e-mail beechem@lhmrba.hh.vanderbilt.edu; phone 615-322-7980; fax 615-322-7236.

‡ The Pennsylvania State University.

§ Vanderbilt University.

|| Present address: Laboratory of Atomic and Solid State Physics and Center for Material Research, Cornell University, Ithaca, NY 14853.

10.1021/bi9829433 CCC: $18.00
Published on Web 03/12/1999

reaction. By use of this double-kinetic approach, it is possible to monitor rotational dynamics of the protein, and thus size, during the refolding reaction. A critical consideration is that the high sensitivity of fluorescence anisotropy permits experiments to be conducted at protein concentrations in the low micromolar concentration range. This capability is essential to avoid association/aggregation effects that often complicate SAXS[1] experiments (*22, 23*).

The α-subunit of tryptophan synthase, αTS, is a particularly interesting candidate for the application of the double-kinetic fluorescence anisotropy experiment. Although the X-ray structure shows αTS to be a single α/*β* barrel structural domain (*24*), the urea-induced equilibrium unfolding reaction involves two stable intermediates (*25*−*27*). The intermediate populated at 3 M urea retains substantial secondary structure and partially excludes its aromatic chromophores from solvent. The intermediate populated at 5 M urea has little or no secondary structure and is only readily detected by proton NMR (*26*) or multiple-wavelength fluorescence measurements (*27*). Kinetic studies reveal a complex process that has been interpreted in terms of both off- and on-pathway intermediates. The off-pathway species are the product of a burst-phase reaction, whereas the latter forms are thought to link multiple unfolded and native conformers through parallel folding channels (*28*). The on-pathway intermediates are thought to be equivalent to the stable intermediate populated at 3 M urea.

Although stopped-flow far-UV CD and FL spectroscopies have provided information on the development of secondary structure and exposure of the tyrosines to solvent, respectively, relatively little is known about the sizes of the transient partially folded forms in αTS. Time-resolved fluorescence anisotropy studies of αTS during the folding reaction offer insights into the apparent radii of both on- and off-pathway intermediates. Additionally, this technique allows structural comparisons between a stable equilibrium intermediate and early kinetic folding intermediates.

MATERIALS AND METHODS

Protein/Sample Preparation. αTS was isolated from the *Escherichia coli* host W3110 (Δ*tonB*−*trp*)BA17*his*$^-$ containing the plasmid pBN55. The protein was purified from the soluble extract as described previously (*29*). Purification was done on a DEAE-52 anion-exchange column (Pharmacia, Piscataway, NJ) eluted with 10 mM potassium phosphate, 4 mM K_2EDTA, and 1 mM DTE, pH 7.8. αTS(1−188) was purified from inclusion bodies as described previously (*30*) with the following modifications. The protein was eluted from the DEAE-52 resin with a 0−300 mM KCl linear gradient in 10 mM potassium phosphate (pH 7.8), 2 mM K_2EDTA, and 1 mM DTE. αTS(1−188) was further purified by sizing chromatography on a G-100 Sephacryl column (Pharmacia). Sample integrity and purity were checked by SDS gel electrophoresis, absorbance, and activity assay (αTS only) (*29*). All folding experiments were carried out in an aqueous buffer containing 10 mM potassium phosphate, 0.2 mM K_2EDTA, and 1 mM DTE or BME at pH 7.8 and 25 °C. ANS was purchased from Molecular Probes (Eugene, OR) and used without further purification. The urea solutions were prepared fresh each day with Ultrapure urea from ICN Biomedicals, Inc. (Aurora, OH). Sample concentrations were determined by absorbance measurements using extinction coefficients of $\epsilon_{278} = 12\,760$ M^{-1} cm^{-1} for αTS, $\epsilon_{277} = 9067$ M^{-1} cm^{-1} for αTS(1−188), and $\epsilon_{370} = 6800$ M^{-1} cm^{-1} for ANS.

Equilibrium Folding Experiments. Steady-state fluorescence experiments under equilibrium folding conditions were carried out on an Aviv ATF105 fluorometer equipped with a Microlab 540B automatic titrator (Hamilton Co., Reno, NV) and computer-controlled Glan-Taylor polarizers. The standard PMT housing was replaced with a thermoelectrically cooled PMT housing (Products for Research Inc., Danvers, MA). Fluorescence spectra between 400 and 600 nm were acquired with vertically polarized excitation and magic-angle detection at approximately 0.2 M increments of the urea concentrations between 0 and ∼8 M urea. The urea concentration was determined by measurement of the index of refraction at 20 °C (*31*) on an Abbe refractometer. Equilibration times were typically >500 s at urea concentrations below 5 M and 300 s above this urea concentration. These time scales are sufficient for completion of >99.5% of the folding/unfolding reaction. The protein concentration was 10 μM.

Time-correlated single-photon counting (TCSPC) experiments under equilibrium folding conditions were acquired as previously described (*20, 21*). Briefly, the doubled output of an argon ion-pumped mode-locked Ti−sapphire laser (Coherent Inc., Palo Alto, CA) provided ∼1 mW of 370 nm excitation at a repetition rate of 2 MHz. This excitation wavelength is near the maximum of the lowest-energy ANS absorption band. Typical counting rates were $\sim 10^3$ cps. The emission monochromator was centered at 450 nm with a bandwidth of 4 nm.

Stopped-Flow Refolding Experiments. Stopped-flow reactions were initiated with a Biologic (Claix, France) SFM-3 stopped-flow module. A solution of denatured protein in 5.4 M urea was diluted 9-fold with ANS-containing buffer to give a final solution of 10 μM αTS and 0.6 M urea. All studies used a 1.5 mm cuvette. Dead times were estimated to be ∼5−10 ms.

To obtain a better understanding of the ANS fluorescence changes during the refolding experiment, instrumentation was assembled to allow for the collection of full steady-state emission wavelength spectra on the millisecond time scale. Fluorescence spectra at a variety of timing intervals (ranging from 1 to 100 ms/spectra) were collected by a fiber-optic coupling of the ANS emission from the stopped-flow cuvette to the entrance slit of an Instruments SA (Edison, NJ) model HR320 0.32 m imaging spectrograph equipped with an intensified diode array optical multichannel analyzer (OMA) (Princeton Instruments, Trenton NJ, model IPDA-512 G/B). The 370 nm excitation light from a Spex Fluorolog2 was

[1] Abbreviations: αTS, α-subunit of tryptophan synthase from *Escherichia coli*; αTS(1-188), fragment of α-subunit of tryptophan synthase comprising residues 1 through 188; ANS, 1-anilino-8-naphthalene sulfonate; BME, *β*-mercaptoethanol; CD, circular dichroism spectroscopy; DTE, dithioerythritol; FL, fluorescence; I1, urea-stabilized equilibrium intermediate of α-subunit of tryptophan synthase populated in 3 M urea; I2, urea-stabilized equilibrium intermediate of α-subunit of tryptophan synthase populated in 5 M urea; I_{BP}, kinetic intermediate of α-subunit of tryptophan synthase populated within the stopped-flow burst phase; K_2EDTA, ethylenediaminetetraacetic acid, dipotassium salt; N, native state; PMT, photomultiplier tube; SAXS, small-angle X-ray scattering; SDS, sodium dodecyl sulfate; SVD, singular value decomposition; TCSPC, time-correlated single-photon counting; U, unfolded state.

coupled to the sample cuvette of the stopped-flow unit via a fused-silica fiber-optic bundle. Typical data set sizes for these experiments were 2 × 500 × 512, reflecting the two polarization states of the emission, 500 ms-resolved spectra, and 512 elements of the OMA reflecting emission wavelengths from ∼355 to 611 nm.

In the double-kinetic experiment, multiple TCSPC fluorescence measurements are performed during a single stopped-flow refolding experiment (*21*). This capability reflects the >6 orders of magnitude difference between the ∼10−20 ns ANS lifetime and the >millisecond time scale of the folding reactions being monitored. Typically, refolding traces were collected for ∼25 s for each syringe push. This refolding time scale was subdivided into approximately 100−120 subregions for the collection of time-resolved anisotropy decay data. Each time region (or slice) thus represents a separate nanosecond TCSPC experiment tagged with the appropriate average refolding time. Between 300 and 600 syringe shots were accumulated in a single experiment with the polarizer rotated every 10 syringe shots. Typical data set sizes were 2 × 120 × 1500 data points, representing the two polarization states, 120 "millisecond-resolved" time slices, and 1500 picosecond/nanosecond-resolved data points obtained for each slice. Counting rates were typically ∼35K cps.

In all equilibrium and stopped-flow experiments, the final protein concentration was less than or equal to 10 μM. For the studies on the 1−188 amino-terminal fragment of αTS, the concentration was kept below 3 μM. At these concentrations, both αTS and the amino-terminal fragment are known to be monomeric (P. Gualfetti, J.A.Z., and C.R.M., unpublished results). The final ANS concentration, unless stated otherwise, was 10 μM.

Data Analysis. Steady-state equilibrium urea denaturation experiments were analyzed by fitting the intensity-weighted average emission wavelength to a two- or three-state denaturation model (*32*, *33*). The intensity-weighted average emission wavelength, or center-of-mass of the emission spectrum, is obtained from

$$\langle\lambda_j\rangle = (\sum I_{i,j}\lambda_i)/(\sum I_{i,j}) \quad (1)$$

where $I_{i,j}$ represents the intensity of the ith wavelength, λ_i, at a particular urea concentration, j, and the summation is over the wavelength index, i. Because differences in integrated intensity, $\sum I_i$, were within a factor of 2 near the transition regions, use of the intensity-weighted average emission wavelength to obtain thermodynamic parameters was considered a good approximation. The strong denaturant dependence of the native baseline precluded obtaining reliable thermodynamic parameters from global fits of the intensity data.

The multidimensional kinetic data sets were analyzed by a variety of methods. Stopped-flow data with multiple wavelength detection were globally analyzed via singular value decomposition (SVD). In addition to providing a more efficient means of globally fitting large two-dimensional data sets, SVD allows one to determine the minimum number of unique components required to represent the data (*34*). The minimum number of significant basis vectors necessary to adequately represent the original data matrix was determined by consideration of the singular values and the autocorrelation of the corresponding basis vectors. The basis vectors representing the time evolution were fit to the minimum number of statistically significant exponentials with the time constants being globally linked for all included basis vectors. The pure ANS spectra associated with distinct bound states were then obtained by the appropriate matrix multiplication of the fit parameters (*34*).

The equilibrium TCSPC anisotropy data were fit to an associative decay model as described previously (*20*). For the double-kinetic anisotropy data, each time slice was analyzed locally using the horizontal and vertical components as for the equilibrium TCSPC data. Thus, using t to describe the ns fluorescence time axis and t_r to describe the refolding time axis, the double-kinetic time-resolved data is described by the following expressions:

$$I_{vv}(t, t_r) = \sum_{i=1}^{N} S_i(t, t_r)[1 + 2r_i(t, t_r)]/3 \quad (2)$$

$$I_{vh}(t, t_r) = \sum_{i=1}^{N} S_i(t, t_r)[1 - r_i(t, t_r)]/3 \quad (3)$$

where N is the number of molecular species (e.g., for free-ANS and αTS-bound ANS, $N = 2$)

$$S_i(t, t_r) = \sum_{j=1}^{n_j} \alpha_j(t_r) \exp[-t/\tau_j(t_r)] \quad (4)$$

and

$$r_i(t, t_r) = \sum_{k=1}^{n_k} \beta_k(t_r) \exp[-t/\phi_k(t_r)] \quad (5)$$

The total intensity is obtained in the usual manner, $I_{vv} + 2GI_{vh}$, where $G = I_{hv}/I_{hh}$ (*19*). In the above expressions $S_i(t, t_r)$ and $r_i(t, t_r)$ are the fluorescence intensity and anisotropy, respectively, for species i. The fluorescence lifetime and rotational correlation time are represented by τ and ϕ, respectively. Thus, the total fluorescence for species i is represented by n_j exponential terms and the anisotropy decay is represented by n_k rotational correlation times. In this manner one obtains α_j, τ_j, β_k, and ϕ_k for each time slice t_r along the refolding time coordinate.

An alternative approach was developed in which the entire data matrix was fit globally by use of a specified kinetic mechanism. In addition to significantly reducing the number of parameters used to describe the data matrix, this approach improves parameter estimation and allows one to directly obtain parameters for the kinetic intermediates themselves. The above expressions for $S_i(t, t_r)$ and $r_i(t, t_r)$ are thus substituted with

$$S_i(t, t_r) = \sum_{I=1}^{n_I} C_I(t_r) s_I(t) \quad (6)$$

and

$$r_i(t, t_r) = \sum_{I=1}^{n_I} C_I(t_r) s_I(t) r_I(t) / S_i(t, t_r) \quad (7)$$

where the subscript I denotes the Ith kinetic intermediate and C_I gives the concentration of I at the refolding time t_r. The fluorescence decay, s_I, and anisotropy decay, r_I, of intermediate I are described by

$$s_I(t) = \sum_{m=1}^{n_m} q_{Im} \exp(-t/\tau_{Im}) \quad (8)$$

and

$$r_I(t) = \sum_{p=1}^{n_p} r_{0Ip} \exp(-t/\phi_{Ip}) \quad (9)$$

.

In this case one optimizes for the parameters q_{Im}, τ_{Im}, r_{0Ip}, and ϕ_{Ip} and the eigenvalues of the system matrix that yields the rate constants. The distinction in this analysis is that the parameters q_{Im}, τ_{Im}, r_{0Ip}, and ϕ_{Ip} now refer to intrinsic properties of the intermediates as opposed to a phenomenological description of the data (see ref 21, pp 45−47 for a more detailed description of this analysis approach).

In all of the least-squares fitting routines the Marquardt−Levenberg algorithm was used (*35*). The instrument response was taken into consideration by iterative reconvolution. All analyses were performed using the Globals Unlimited (Urbana, IL) (*36*) and Savuka (D. Lambright and O. Bilsel, personal communication) software packages.

RESULTS

The seven tyrosine residues in αTS do not provide sufficient fluorescence intensity to permit the application of the double-kinetic technique to the measurement of rotational correlation times in the millisecond refolding time range. Also, the excited-state lifetime of tyrosine, 3−5 ns, is not ideal for measurement of protein global rotational motions expected to occur in the 10−20 ns time range. Therefore, 1-anilino-8-naphthalene sulfonate, ANS, was included in the refolding buffer to serve as a bound extrinsic probe of protein dynamics. Partially folded forms of proteins readily bind ANS, resulting in a large blue shift in the emission maximum and a dramatic increase in intensity (*37*). These changes in fluorescence properties presumably reflect binding of ANS to nonpolar surfaces exposed in partially folded proteins.

Equilibrium Folding Studies

To provide a framework for interpreting both the ANS emission spectra and the time-resolved anisotropy data for kinetic folding experiments on αTS, corresponding data for the urea-induced equilibrium unfolding were also collected. The urea-induced unfolding of αTS can be described by a four-state model, N ⇄ I1 ⇄ I2 ⇄ U (*25*, *27*, *38*). The equilibrium intermediate I1 is a partially unfolded form that is highly populated near 3 M urea, and I2 is an unfoldedlike form that is highly populated near 5 M urea. The unfoldedlike nature of the I2 equilibrium intermediate renders it spectroscopically very similar to U by most optical methods.

Steady-State ANS Fluorescence. A series of emission spectra of ANS in the presence of αTS and increasing urea concentrations are shown in Figure 1A. The strong emission near 470 nm in the absence of denaturant demonstrates that ANS binds to the native conformation. An independent

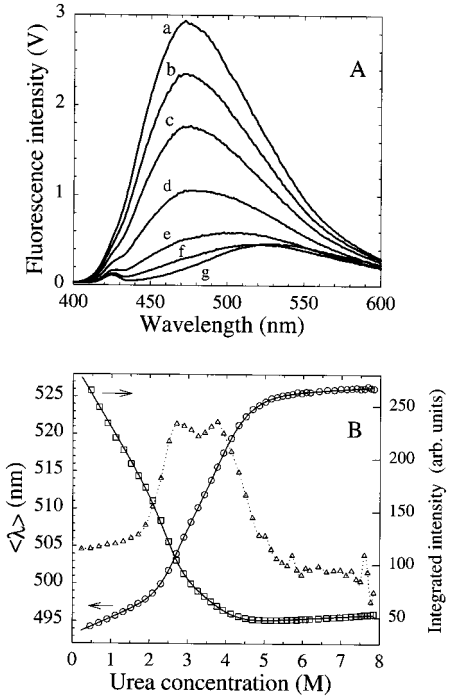

FIGURE 1: Equilibrium titration of 2.5 μM WT αTS with urea in the presence of 10 μM ANS. Excitation was at 370 nm with a bandpass of 2.5 nm. (A) Representative fluorescence spectra at (a) 0.0, (b) 0.90, (c) 1.71, (d) 2.50, (e) 3.26, (f) 3.93, and (g) 7.60 M urea. The full data set consisted of 48 spectra at increasing urea concentrations between 0 and 7.80 M urea. All samples contained 10 mM potassium phosphate, 0.2 mM K_2EDTA and 1 mM βME and were equilibrated at 25 °C. The spectra are not corrected for monochromator/PMT efficiency. The small peak near 425 nm is due to Raman scattering from water. (B) Intensity-weighted average emission wavelength (○, left vertical axis) and integrated emission intensity (□, right vertical axis) calculated from the same data set as in panel A. The averaging and integration were performed over the 400−600 nm wavelength range. The smooth line represents a fit to a three-state denaturation curve. Fit parameters are shown in Table 1. The dotted line with triangles (arbitrary vertical axis) is the first derivative of the average-emission wavelength curve.

titration of native αTS with ANS yields a K_d of 46 ± 5 μM, assuming a single-site binding model (data not shown). The structural resemblance of ANS and the natural substrate for αTS, indole-3-glycerol phosphate, may account for this relatively tight binding to the native conformation (*37*).

As the urea concentration increases, the emission intensity decreases (Figure 1) and, between 2 and 5 M urea, shifts to the red (Figure 1B). Although subtle, there is a small inflection in the average emission wavelength transition curve near 3 M urea that reflects the presence of an intermediate state. The first-derivative plot exhibiting maxima near 2.7 and 3.8 M urea more closely illustrates this behavior (Figure 1B). The average emission wavelength data were fit to both two- and three-state equilibrium models. The three-state nature of the denaturation was confirmed by comparison of the reduced-χ^2 values ($\chi^2_{2state}/\chi^2_{3state}$ = 3.1). These data suggest that both the native and intermediate forms of αTS can bind ANS. Assuming a linear dependence of the apparent free energy of folding on the urea concentration, the free energies $\Delta G°_{NI}$ and $\Delta G°_{IU}$ for αTS in the presence of 10 μM ANS are very similar to the N ⇄ I1 and I1 ⇄ I2 transitions in its absence (Table 1). The excellent agreement shows that ANS does not significantly perturb the thermodynamic properties of the multistate equilibrium unfolding

Table 1: Thermodynamic Parameters for the Urea-Induced Unfolding of αTS[a]

	$\Delta G°(H_2O)_{N-I1}$ (kcal mol^{-1})	m_{N-I1} (kcal mol^{-1} M^{-1})	$\Delta G°_{I1-I2}(H_2O)$ (kcal mol^{-1})	m_{I1-I} (kcal mol^{-1} M^{-1})
αTS (ANS FL)[b]	6.24 (0.3)	2.38 (0.2)	5.16 (0.2)	1.35 (0.04)
αTS (Tyr FL)[c]	6.13 (0.1)	2.36 (0.05)	5.15 (0.37)	1.34 (0.09)
αTS (CD)[d]	6.6 (0.1)	2.4 (0.05)	4.6 (0.4)	1.1 (0.1)

[a] The free energy change in the absence of urea, $\Delta G°(H_2O)_{XY}$, and the dependence of the free energy change on the denaturant concentration, m_{XY}, were calculated from $\Delta G° = \Delta G°(H_2O) - m_{XY}$[urea], as described elsewhere (*32, 65*). Values in parentheses denote one standard deviation as determined from an uncorrelated error analysis. [b] Values determined by monitoring ANS fluorescence. The intensity-weighted average emission wavelength of ANS fluorescence was fit to a three-state denaturation model (*32, 33*). [c] Values obtained by global analysis of tyrosine fluorescence between 295 and 400 nm in the absence of ANS. Although the values are from a fit to a four-state denaturation model, only the values for the first two transitions, comparable to those observed by ANS, are shown. [d] Values obtained by global analysis of CD between 215 and 300 nm in the absence of ANS (*27*). These values are from a fit to a four-state denaturation model. However, only the values for the first two transitions, comparable to those observed by ANS, are shown. The full analysis is reported elsewhere (*27*).

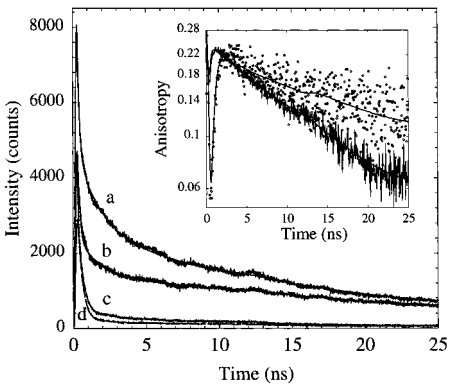

FIGURE 2: Time-correlated single photon counting traces acquired under equilibrium folding conditions with 10 μM αTS and 10 μM ANS. Other conditions are as in Figure 1. The vertical and horizontal polarization components of the ANS excited-state decay are shown at 0 M (a, vertical; b, horizontal) and 3 M urea (c, vertical; d, horizontal) upon excitation with 370 nm vertically polarized light. The fast component corresponds to the decay of unbound ANS. The corresponding calculated anisotropy curves at 0 and 3 M (solid and dotted trace, respectively) are also shown (inset). The smooth lines represent fits to the associative model described in the text.

reaction for αTS. The failure to detect the I2 intermediate near 5 M urea implies either that this species does not bind ANS or that the binding of ANS competes ineffectively with binding of urea (*39*).

Time-Resolved Anisotropy. Time-resolved anisotropy experiments probing the ANS excited-state decay in the presence of αTS were performed at six different urea concentrations between 0 and 3.5 M urea. Representative decay profiles are shown in Figure 2. These data were fit by the associative model described above using a single rotational correlation time and two lifetimes for the bound ANS. Free ANS has a lifetime of approximately 260 ps and a rotational correlation time of ~100 ps. Using the unique capabilities of the double-kinetic apparatus, the fluorescence contribution of these fast free ANS components can be completely "stripped away" from the ANS bound-state signals during the refolding reaction. For instance, 2 ns after the laser pulse, the bound signal is magnified over the free signal by ~200×, and 5 ns after the laser pulse a factor greater than a million times (see ref *21*, pp 41−42 for a representative calculation). Hence, the double-kinetic instrument provides a unique manner to probe bound-state ANS complexes even in the presence of a dominating (in terms of population) free ANS component. The bound-state ANS signal is composed of two lifetime components, of 4−7 ns and 13−20 ns, depending on the solution conditions. Both of the bound-state ANS lifetimes were found to be associated with a single protein rotational correlation time (see Table 2). The free ANS was represented with a single lifetime and single rotational correlation time. Inclusion of additional correlation times for the bound ANS did not improve the quality of the fits. The urea dependence of the fit parameters is shown in Figure 3.

Table 2: Bound ANS Parameters Obtained from Global Analysis of the Double-Kinetic Data for αTS at 0.6 M Urea[a]

	q_{fast}[b]	τ_{fast} (ns)[c]	q_{slow}[d]	τ_{slow} (ns)[e]	r_o[f]	ϕ[g] (ns)	R_h[h] (Å)
I_{BP}	1.80	7.24	1.30	20.0	0.217	16.3	26.0
I1	1.19	4.10	1.59	17.0	0.207	25.2	30.1
N	1.00	5.12	1.00	18.1	0.261	16.0	25.9

[a] Values were obtained from a global analysis along both the refolding (milliseconds to seconds) and TCSPC (nanoseconds) time axes of the data shown in Figure 5. Fits along the TCSP*C* axis were to the associative model described in Materials and Methods; fits along the refolding time axis were to the kinetic model in Figure 7. The fits assumed that the intermediates along the various channels at a given stage had identical properties. For example, I1 represents the properties of the $I1_a$, $I1_b$, $I1_c$, and $I1_d$ kinetic intermediates. The free ANS was described with a relative intensity of $q_{BP} = 49\,192$, $q_{I1} = 49\,790$, and $q_N = 63\,711$ counts for the I_{BP}, I1, and N states, respectively. The excited-state lifetime of free ANS, 266 ps, was linked for all states and the rotational correlation time was fixed at 100 ps. The time slices were normalized to account for the different accumulation times for each time slice. The two adjustable refolding kinetic parameters were $k_{IBP\rightarrow I1} = 1.5 \pm 0.1$ s^{-1} and $k_{I1c\rightarrow I1b} = 0.08 \pm 0.01$ s^{-1} (Figure 7). Kinetic parameters corresponding to the slower refolding phase were fixed at $k_{I1d\rightarrow I1c} = 1/44$ s^{-1} and $k_{I1a\rightarrow I1b} = 1/250$ s^{-1}. [b] Fluorescence intensity of the faster bound ANS excited-state decay component given as a ratio relative to that of the native form (3114 counts). [c] Lifetime of the faster bound ANS excited-state decay. [d] Fluorescence intensity of the slower bound ANS excited-state decay component given as a ratio relative to that of the native form (6059 counts). [e] Lifetime of the slower bound ANS excited-state decay. The lifetime of the native state was fixed at 18.1 ns based on interpolation of the equilibrium data shown in Figure 3 to a final urea concentration of 0.6 M. [f] Initial anisotropy of the bound ANS anisotropy decay. [g] Rotational correlation time of the bound ANS anisotropy decay. The value for the rotational correlation time for *N* was fixed at 16.0 ns based on interpolation of the equilibrium data in Figure 3 to a final urea concentration of 0.6 M. [h] Calculated hydrodynamic radius at 0.6 M urea, assuming a spherical shape and viscosity of 0.907 cp.

The fast and slow components of the ANS excited-state decay (Figure 2) and the associative rise/fall anisotropy profile (Figure 2, inset) arise from the very large differences in the excited-state lifetime and rotational correlation time between ANS free in solution (≪1 ns) and ANS bound to protein (>1 ns). A significant increase in the excited-state lifetime of ANS upon binding to hydrophobic regions of proteins has been observed for many other proteins (*37*). The anisotropy calculated from the vertical and horizontal components of the excited-state decay (Figure 2, inset) demonstrates how the double-kinetic instrumentation can make use of the large lifetime change to "decouple" the free ANS signal from the bound-state signal. Even without rigorous data analysis, one can essentially just "wait" for

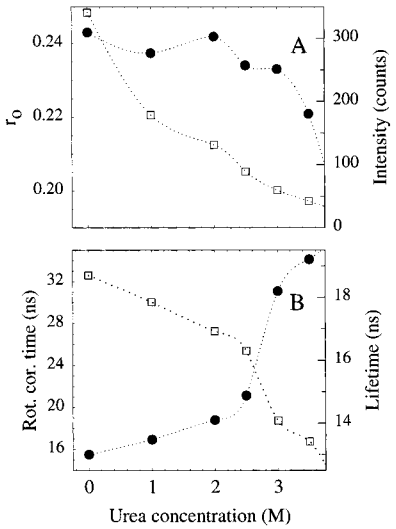

FIGURE 3: Urea concentration dependence of the parameters obtained from fits of the TCSPC traces under equilibrium folding conditions. The amplitude (panel A, □; right axis), excited-state lifetime (panel B, □; right axis), initial anisotropy (panel A, ●; left axis) and rotational correlation time (panel B, ●; left axis) associated with the longer lifetime component of ANS bound to αTS are shown. The behavior of the longer lifetime component was the focus of the present study because it makes the dominant contribution to the rotational correlation time of the bound ANS. The shorter lifetime component may reflect alternative ANS binding sites or excited-state dynamics of the bound ANS (*37*). The αTS and ANS concentrations were each 10 μM. All other conditions were as in Figure 1.

the free ANS signals to decay away (e.g., 4 ns after the laser pulse) and generate an anisotropy signal associated with only the bound state (see anisotropy data at >4 ns of Figure 2, inset). Full associative-type anisotropy decay analysis (solid lines in Figure 2 inset) allows the decoupling to be performed on a quantitative basis, even at short time scales. The rotational correlation time recovered from the associative anisotropy fits of the bound ANS state is consistent with the global Brownian rotational correlation function of the entire protein. The rotational correlation time in the absence of urea, 14.0 ± 0.5 ns, is consistent with that expected for a spherical molecule of molecular mass 29 kDa and a typical hydration of 0.2 g of H_2O/g (*19*). Using a value of 0.89 cp for the viscosity of water at 25 °C (*40*), this rotational correlation time corresponds to a hydrodynamic radius of 24.7 Å (see Discussion for a more detailed calculation of hydrodynamic properties).

The amplitude of the bound ANS signal decreases at higher urea concentrations and is significantly diminished by 3.5 M (Figure 1A), where I1 still represents a substantial fraction, ~45%, of the αTS population (*27*, *41*). This behavior most likely results from competitive inhibition of ANS binding to αTS by urea (*39*). Consistent with this explanation are the results of stopped-flow refolding studies (see below), which confirm that ANS bound to the I1 species that transiently exists under strongly folding conditions has a higher fluorescence quantum yield than when bound to N. The inability of ANS to bind to αTS at high urea concentrations precluded extension of denaturation curves above 3.5 M.

As the urea concentration is increased, a transition can be seen in the excited-state lifetime and rotational correlation time between 2 and 3 M urea (Figure 3B). This region corresponds to the N ⇄ I1 transition observed for αTS in the absence of ANS by other optical techniques (*27*, *42*). The nearly constant value of the initial anisotropy, r_0, in the same region (Figure 3A) suggests that the absorption and emission electronic transition moments of the bound ANS for the N and I1 species are probably similar. The increase in rotational correlation time near 3 M urea is consistent with an increase in the volume of the protein upon partial denaturation to the I1 state (*43*). Because the population of the native state by 3.5 M urea is <5% and the quantum yield of ANS bound to N is less than when bound to I1 (see below), the bias introduced by not being able to discriminate their rotational correlation times is not likely to be significant. The values of 31 and 34 ns at 3.0 and 3.5 M urea, respectively, correspond to hydrodynamic radii of approximately 30.7 and 31.7 Å, assuming a spherical shape and a solvent viscosity of 1.014 and 1.047 cp, respectively (*40*).

The gradual increase in the rotational correlation time in the native baseline region from 0 to 2 M urea (Figure 3B) is greater than that expected simply from viscosity differences. Possible explanations include local unfolding reactions or changes in the hydration state of αTS at increasing urea concentration. Because absorbance and circular dichroism data suggest that αTS remains well-folded in this region (*27*, *28*, *41*), the latter explanation is more likely.

Stopped-Flow Kinetic Folding Studies

Steady-State Fluorescence. Stopped-flow refolding experiments of αTS in which the full ANS fluorescence spectra were collected on the millisecond time scale (see methods) are summarized in Figure 4. At the earliest observation times following mixing (~10 ms), the ANS emission spectrum is considerably blue-shifted and more intense (Figure 4A, solid line) relative to that of unbound ANS in solution (Figure 4A, dotted line). The 470 nm emission maximum of the burst-phase intermediate, I_{BP}, is very close to that observed for ANS bound to the N and I1 equilibrium species (Figure 1). This similarity suggests that similar ANS binding sites are likely to exist for I_{BP}, an off-pathway intermediate, the on-pathway intermediate I1, and the native state. The ~20 ms ANS emission spectrum evolves with an ~1 s time constant to a spectrum with a similar peak maximum but approximately 5% reduced intensity (Figure 4). The increase in the free ANS emission at increasing refolding times gives rise to the increase in the intensity-weighted average emission wavelength (Figure 4B). Refolding experiments out to several hundred seconds (not shown) showed a continual decrease in the emission intensity while maintaining a relatively constant blue-shift.

Independent analysis of the data at each wavelength suggested that the data are statistically best fit to two exponential functions with no detectable wavelength dependence of the time constants. Confirming this finding, analysis of the multiwavelength data by SVD indicated that the data are adequately represented by two spectral components, as judged by the singular values and the autocorrelation of the corresponding basis vectors. The time constants for the folding reaction ($\tau_1 = 0.5 \pm 0.1$ s, $\tau_2 = 7.5 \pm 1.0$ s) were obtained by globally fitting the two significant basis vectors representing the time evolution. These time constants agree closely with those obtained by monitoring tyrosine fluorescence and far-UV CD in the absence of ANS (*28*). The

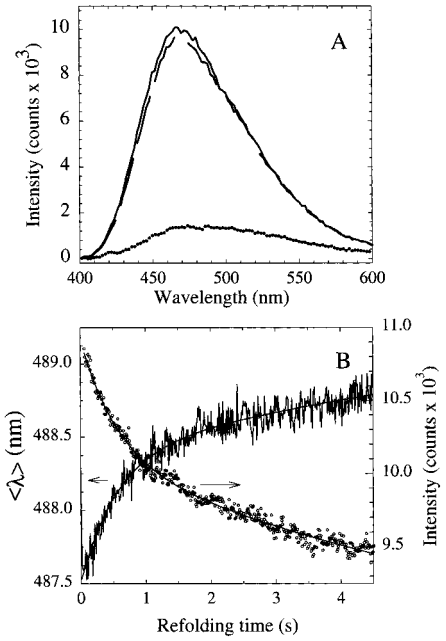

FIGURE 4: (A) ANS emission spectra at various times following initiation of refolding: 20 ms (solid line) and 4.5 s (dashed line). The pre-shot spectrum (dotted line), representing the αTS/ANS solution at 5.4 M, urea is also shown. Refolding was initiated by dilution of urea from 5.4 to 0.6 M. The final αTS and ANS concentrations are as in Figure 1. The emission spectra are not corrected for the monochromator and PMT efficiency. (B) Intensity-weighted average emission wavelength between 400 and 600 nm (solid line) and intensity at 470 nm (dotted line) versus refolding time. The smooth solid lines represent fits to a biexponential decay function. The intensity at 470 nm was fit with $y = 8588 + 741 \exp(-t/0.50) + 1569 \exp(-t/7.5)$, and the average emission wavelength was fit with $y = 489.5 - 0.86 \exp(-t/0.55) - 1.14 \exp(-t/10.)$.

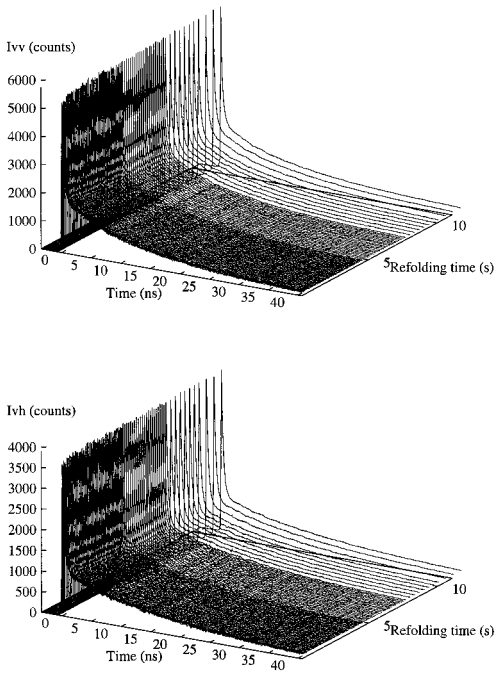

FIGURE 5: Representative double-kinetic data set showing the vertical (top panel) and horizontal (bottom panel) components of the bound ANS excited-state decay during the first 5 s of refolding. The αTS and ANS concentrations were each 10 μM. The data set is the average of approximately 300 refolding events. The number of counts in each time slice has been normalized by the length of its time window. The final urea concentration was 0.6 M. All other conditions were as in Figure 1.

quantitative agreement of these time constants [and more extensive data using these same techniques (*44*)] provides further confirmation that ANS does not noticeably perturb the folding of αTS (*45*).

Time-Resolved Fluorescence. A representative raw double-kinetic data set for αTS along the two pertinent time axes is shown in Figure 5. Similar to the equilibrium TCSPC data, the vertical and horizontal components each exhibit a fast-decaying component, corresponding to ANS in solution, and a substantially longer decay corresponding to ANS bound to αTS. Data from each time slice were treated as a separate time-resolved anisotropy experiment with a stopped-flow time tagged to it. The associative model used to fit the bound ANS signal consisted of a single correlation time and two lifetimes. As found for the equilibrium folding data, inclusion of additional rotational correlation times did not yield statistically significant improvements in the fit. The free ANS was represented by a single lifetime of ~300 ps and a single correlation time fixed at 100 ps. Fit parameters corresponding to the amplitude, longer excited-state lifetime, initial anisotropy, and rotational correlation time of bound ANS as a function of refolding time are presented in Figure 6, panels A−D, respectively.

The refolding time dependence of the rotational correlation time (Figure 6D) is particularly interesting. First, the maximum rotational correlation time of ~22 ns during refolding suggests that kinetic intermediates of αTS are relatively compact on the greater than milliseconds refolding

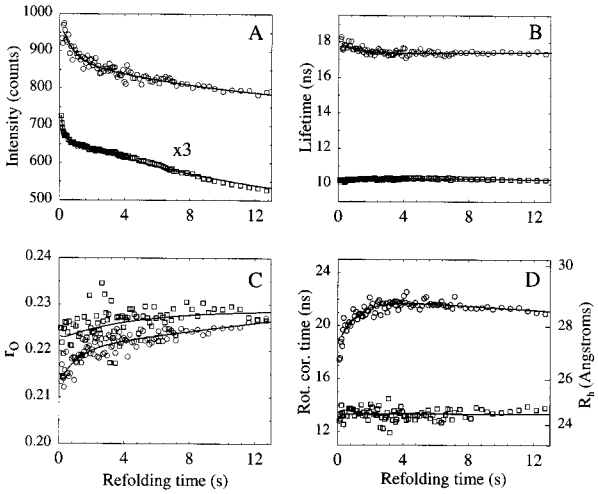

FIGURE 6: Fit parameters obtained from an independent analysis of TCSPC experiments at each refolding time slice. The amplitude (A), excited-state lifetime (B), initial anisotropy (C), and rotational correlation time (D) of ANS bound to αTS (○) and αTS(1−188) (□) are shown. Only the parameters associated with the longer lifetime of the bound ANS are shown for αTS. The smooth solid line represents an independent fit of each trace to a biexponential decay function. The right vertical axis in panel D is the hydrodynamic radius calculated, assuming a spherical shape, from the rotational correlation time obtained from the left vertical axis. The scale on the right in panel D is nonlinear and varies as the cubic root of the left vertical axis.

time scale. Because the rotational correlation time depends linearly on the volume, the maximally 70% greater volume suggests that the hydrodynamic radius must be within 20% that of the native form even at the earliest detectable stages of folding. A second noteworthy feature is the nonmonotonic

dependence of the rotational correlation time on refolding time. Within 50 ms, the rotational correlation time of αTS is ∼17 ns. This value *increases* with a time constant of ∼1 s to approximately 22 ns before decreasing to ∼19 ns with a time constant of ∼10 s. Preliminary measurements recorded on a time scale of several hundred seconds indicated that the rotational correlation time continued to decrease on a longer refolding time scale than the ∼1 s and ∼10 s phases (data not shown). This result is consistent with stopped-flow CD, absorbance, and total fluorescence measurements where refolding phases with ∼40 and ∼300 s time constants have been observed (*28*). Aggregation as a source of the transient increase in the rotational correlation time was ruled out by obtaining the same results when αTS was diluted 3-fold to 3.3 μM.

The excited-state lifetime of ANS bound to αTS, similar to the rotational correlation time, displays a nonmonotonic dependence on refolding time (Figure 6B). The lifetime decreases to a minimum after ∼2 s before slightly increasing at longer times. Because the excited-state lifetime of ANS has been shown to depend on the hydrophobicity of the local environment (*37*), this behavior might reflect the availability of more hydrophobic regions for the binding of ANS in the off-pathway burst-phase intermediate relative to the on-pathway I1 intermediate. The lifetime of the free ANS in solution did not change as a function of refolding time and was typically ∼300 ps.

The bound ANS amplitude (Figure 6A) and initial anisotropy (Figure 6C) show a gradually decreasing and increasing trend, respectively, with respect to refolding time. The decrease in the bound ANS fluorescence intensity can be attributed to the interplay of two factors: a change in the quantum yield of bound ANS relative to that for the burst-phase intermediate and a change in the fraction of ANS bound to αTS. That the binding of ANS to αTS is reduced at longer refolding times is supported by the increase in the free ANS amplitude (data not shown). Delineation of the relative quantum yield of ANS bound to different kinetic intermediates necessitates a global analysis and is discussed below.

The complexity of the kinetic model for αTS (*28*), which postulates four channels each with on- and off-pathway intermediates, dictates that the recovered fluorescence parameters will reflect the composite properties of several species. To extract the optical and hydrodynamic properties of individual species, a global analysis along both time domains and in the framework of the proposed refolding mechanism was performed. By necessity, the folding model was simplified by assuming that the structural and optical properties of the set of four burst-phase intermediates, I_{BP}, were identical. The same assumption was made for the subsequent set of I1 intermediates. Partial justification for this assumption is provided by the global analysis of the CD refolding data, which yielded very similar optical properties for the I1 intermediates (*28*). These data were fit to a nine-species kinetic mechanism based on the model shown in Figure 7. Because the $I_{BPx} \rightarrow U/I2_x$ rate is much slower than the $U/I2_x \rightarrow I1_x$ rate, the $U/I2_x$ species are not significantly populated and, therefore, not explicitly included in the model. The results of the global fit of the entire data set to this mechanism are shown in Table 2. The fit to the four-channel model was superior, based on comparison of reduced-χ^2 values, to a three-state sequential mechanism without parallel channels.

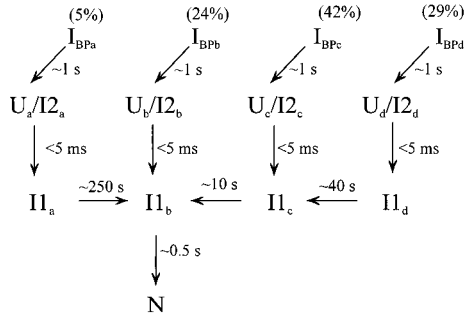

FIGURE 7: Kinetic folding model of αTS at strongly folding conditions. The model describes the stages following formation of the burst phase intermediate, I_{BP}. The populations of the kinetic intermediates in the global analysis of the double-kinetic data were based on this approximation to the full kinetic mechanism (*28*). The values in parentheses denote the population of each refolding channel. $U_x/I2_x$ represents a composite kinetic species that reflects the very rapid interconversion of these two forms under strongly folding conditions. The exclusion of the minor native component included in the complete mechanism does not significantly affect these results because its maximal population on the time scale of the double-kinetic data analyzed (up to approximately 13 s) is approximately 2%, within error of the estimates of the channel populations. In comparison, the maximal population of the dominant native form 13 s into the refolding reaction is approximately 50%.

The global analysis permits a delineation of the rotational correlation times, lifetimes, and relative quantum yields of the refolding intermediates of αTS. Consistent with independent analysis of each time slice of the double-kinetic experiment, the rotational correlation time of the burst-phase intermediate, 16.3 ns, is less than that of the subsequent on-pathway I1 intermediate. The 25.2 ns rotational correlation time obtained for the I1 intermediate is slightly greater than the maximum rotational correlation time observed in the local analysis, ∼22 ns. This arises because the global analysis accounts for the formation of an ∼20% population of native species with an ∼1 s refolding time constant via the minor, fast-folding channel (Figure 7, channel B) (*28*). Independent analysis of the time slices is unable to discriminate between the rotational correlation times of the native, I1, and I_{BP} species, reporting instead a weighted average. In a similar manner, the global analysis highlights that the ∼19 ns rotational correlation time measured 12 s into the refolding reaction reflects a quantum-yield weighted average of the rotational correlation times of native (∼60%) and I1 (∼40%) species. Also, the increase in the free ANS concentration is most pronounced upon interconversion of I1 to the native form (footnote *a* in Table 2).

In an effort to gain insights into the structural implications of the observed rotational correlation times for the folding intermediates of αTS, analogous studies were carried out for a fragment comprising the first 188 residues, αTS(1−188). This fragment is known to adopt a stable fold (*46*) and has recently been found to preserve several of the kinetic folding reactions detected in the full-length protein (J.A.Z. and C.R.M., unpublished data). A notable exception is the absence of a small amplitude refolding phase on the ∼300 s time scale. Previous comparisons between this fragment and the full-length protein had led to the suggestion that the equilibrium intermediate (*46*) and the kinetic intermediate preceding formation of the native form of αTS (*42*, *47*) have

a folded amino-terminal domain, residues 1−188, and an unfolded carboxy-terminal domain, 189−268. Although more recent results suggest that these folding units are associated in I1 (*30, 48*), the present experiments offer another test of this hypothesis.

The refolding time dependence of the ANS amplitude, excited-state lifetime, initial anisotropy, and rotational correlation time for ANS bound to αTS(1−188) are shown in Figure 6. These parameters were obtained from individual fits of each time slice to an associative decay model with a single lifetime and single correlation time for the bound ANS signal and also for the free ANS signal (free ANS parameters are not shown). The rotational correlation time (Figure 6D) and bound ANS lifetime (Figure 6B) exhibit the most significant differences between αTS(1−188) and αTS. The greater rotational correlation time for the full-length protein relative to the fragment after 20 ms of refolding (18 versus 13 ns) implies that the two folding units of αTS are interacting at the earliest detectable stage in folding, i.e., in I_{BP}. The absence of an increase in the rotational correlation time for αTS(1−188) during refolding reveals that αTS(1−188) quickly refolds into an overall conformation with Brownian rotational dynamics (and hence hydrodynamic radius) very similar to its final native state. The two folding units of full-length αTS, however, clearly undergo a more complex folding pattern, with intermediate states that are expanded with respect to the hydrodynamic radius of either final native state.

The longer bound ANS excited-state lifetime for the full-length protein relative to that of the fragment protein (Figure 6B) is also consistent with the two folding units interacting in the burst-phase species for αTS. This result is also consistent with increased quenching from greater solvent exposure of the bound ANS in the fragment, perhaps reflecting a more open structure. The binding sites for ANS in αTS may include contributions from both the 1−188 and 189−268 folding units. The reduced amplitude for ANS bound to the early intermediates of αTS(1−188) (Figure 6A) lends additional support to this conjecture.

DISCUSSION

The results of time-resolved fluorescence anisotropy experiments on αTS have provided a measure of the compactness of a pair of early refolding intermediates and a highly populated equilibrium intermediate. Comparisons among these forms and with the native form provide useful insights into the contraction of the conformational space available to αTS during folding.

Structural Implications for the Native State and the I1 Equilibrium Intermediate. The results of time-resolved anisotropy studies of the native conformation of αTS in the absence of denaturant are consistent with a highly spherical shape. The hydrodynamic radius of 24.7 Å calculated from the rotational correlation time using the Stokes−Einstein equation (*19*) is in good agreement with the value expected for a protein of this size. An approximately spherical shape for native αTS is also expected on the basis of the crystal structure of the highly homologous αTS from *Salmonella typhimurium* (*24*). The ratios of the inertial axes calculated using the heavy atoms in the crystal structure, 1.0:1.2:1.5, are consistent with a fairly spherical α/β barrel topology with the smallest moment of inertia aligned along the axis of the barrel. Modeling of the hydrodynamic properties of αTS using the bead method (*49*−*52*) without a hydration shell gives rotational diffusion coefficients with a ratio of 1.00: 1.11:1.25 and corresponding rotational correlation times of 10.3, 10.3, 11.0, 11.6, and 11.7 ns. These rotational correlation times are approximately 20% less than the experimentally observed value, most likely reflecting a contribution from the hydration layer. Hydrodynamically coupling all water molecules whose oxygen atoms are within 3.1 Å of the protein surface results in closer agreement with the observed rotational correlation time (τ_{calc} = 13.2−14.8 ns versus τ_{obs} = 14 ns).

The small but significant increase in the rotational correlation time in the native baseline region, 0−2 M urea (Figure 3B), most likely reflects the binding of urea to the surface of αTS (*53*). This conclusion is supported by the absence of changes in secondary and tertiary structure in this region (*41*). The binding of urea to the equilibrium intermediate, I1, probably also explains why the estimated radius at 3 M urea, ∼32 Å (Figure 3B), is larger than that for the same species detected in the kinetic refolding experiment at 0.6 M urea, 30.1 Å (Table 2). Molecular dynamics simulations explicitly including urea suggest that the denaturant can form a gradient near the surface of the protein (*54*) that could alter its hydrodynamic properties.

Structural Implications for the Kinetic Intermediates of αTS. The rotational correlation times observed during the refolding of αTS indicate that the kinetic intermediates I_{BP} and I1 of αTS are relatively compact. Their corresponding apparent hydrodynamic radii (Table 2; Figure 6D, right axis) are within 20% that of the native state under the same conditions. Consistent with this significant narrowing of the conformational search space, these intermediates possess approximately 50% of the native state secondary structure content and bury considerable hydrophobic surface area (*28, 55*). These properties of the early kinetic intermediates are reminiscent of the more commonly studied acid-induced partially folded equilibrium forms of other proteins, referred to as molten globules (*18, 22, 43, 56, 57*).

Additional insights into the interaction of the hypothesized folding units of αTS, residues 1−188 and 189−268, can be obtained from comparison of the time-resolved anisotropy data for αTS with those of the αTS(1−188) fragment. The differences in volume and bound ANS lifetime are consistent with interaction of these folding units in the off-pathway burst-phase species. Interestingly, molecular dynamics simulations with a lattice model representation of αTS (*58*) indicate a contribution of the structurally less organized carboxy-terminal folding unit to the stabilization of the more structured amino-terminal folding unit in an early (off-pathway) intermediate. Because differences in rotational correlation time between αTS and αTS(1−188) are accentuated on the >1 s refolding time scale, this interaction is maintained in the subsequent on-pathway intermediate. The prominent difference in the apparent hydrodynamic radii between the off-pathway burst-phase intermediate, I_{BP}, and the on-pathway I1 intermediate (Figure 6D; Table 2), however, is accompanied by only modest changes in the far-UV ellipticity (*28, 59*). A possible explanation for these observations might involve an unfavorable docking of the carboxy-terminal folding unit with the amino-terminal unit

in I_{BP}, necessitating a significant rearrangement of the carboxy-terminal folding unit to obtain the correct orientation.

Origin of the Nonmonotonic Refolding Time Dependence of the Correlation Time. The increase of the rotational correlation time of αTS and subsequent gradual decrease with increasing refolding times, i.e., the nonmonotonic behavior, involves a contribution from both folding units of the protein as evidenced by the absence of a similar trend for αTS(1−188). This refolding time dependence could arise from several factors. One possibility is that the carboxy-terminal folding unit is only partially organized in the off-pathway burst-phase intermediate, acquiring increased structure and hydrodynamic volume upon interconversion to I1. Thus, the smaller observed apparent radius of I_{BP} might primarily reflect the motion of the more highly organized portions of αTS that bind ANS. Incorrectly folded structures with relatively unstructured regions of the carboxy-terminal folding unit were observed in simulations of the folding of αTS (*58*). The burial of hydrophobic surface area for the interconversion of I_{BP} to I1, as inferred from the denaturant dependence of the associated rate constant (*28*), is consistent with this hypothesis.

An alternative possibility, however, is that the carboxy-terminal region contains significant secondary structure in I_{BP}. In this case, a difference in shape between the burst-phase intermediate and I1 might be responsible for the nonmonotonic behavior of the rotational correlation time. One might suppose, for example, that the initial collapse is nonspecific, resulting in a highly spherical shape. If the subsequent intermediate in the folding of αTS, I1, requires an open, extended fold, an increase in the observed rotational correlation time might result if the reporting probe molecule is suitably oriented. However, it is not clear if the formation of a more asymmetric structure can be reconciled with increasing burial of hydrophobic surface area in I1. Future experiments will aim to address the shape of these compact structures.

The striking nonmonotonic behavior of the rotational correlation time obtained from the double-kinetic studies of αTS curiously parallels that for dihydrofolate reductase (DHFR) from *E. coli* (*20*). For both of these proteins, calculations (*60, 61*) and fragmentation studies (*46, 62, 63*) have demonstrated that isolated fragments of the full-length protein can adopt stable, folded structures. Hydrogen exchange pulse-labeling NMR (*5*), tryptophan anisotropy (*20*), and mutagenesis (J. C. O'Neill and C. R. Matthews, unpublished results) studies of DHFR point to the early formation of a well-packed central β-sheet for the burst-phase intermediate concomitant with a relatively loosely packed adenine binding domain. In the subsequent kinetic phase, which buries significant hydrophobic surface area, an increase in the rotational correlation time of ANS bound to DHFR is observed together with the first evidence of nativelike packing of W74/W47 in the adenine binding domain. The nonmonotonic refolding time dependence of the bound ANS rotational correlation time for both αTS and DHFR suggests that this common phenomenon may originate from the subsequent accumulation of structure around a rapidly formed, stable and highly structured folding unit. In analogy to proposals for the transition states of several small proteins with two-state folding kinetics (*64*), the early intermediates observed by stopped-flow techniques may be better described structurally as nonuniform in packing and organization rather than nonspecifically collapsed.

Comparison of Kinetic and Equilibrium Intermediates of αTS. The kinetic intermediate populated with ∼1 s time constant, I1, has been suggested to correspond to the urea-stabilized equilibrium intermediate (*28*). Consistent with this hypothesis, the rotational correlation time measurements indicate comparable hydrodynamic radii between this intermediate and the I1 equilibrium intermediate, ∼32 Å. Additionally, the rotational correlation time of the burst-phase species, I_{BP}, is less readily reconciled with those of the equilibrium intermediate (Table 2). These transient measurements of the intermediates of αTS suggest that consideration of the effect of the denaturing solvent in equilibrium experiments may be important in measurements of the compactness of equilibrium intermediates (*14*).

Relationship to Other Protein Folding Studies. Studies of the early folding intermediates of myoglobin by SAXS (*12*), α-lactalbumin by light-scattering (*14*), and αTS and DHFR (*20*) by time-resolved anisotropy reveal relatively compact structures having radii within ∼20% that of the native form. These compact structures also typically exhibit a burst-phase amplitude by CD, indicating that the collapse occurring within the stopped-flow burst-phase time scale (<5 ms) is accompanied by formation of significant secondary structure. These early compact structures in which the conformational search space is drastically reduced, either are seen to decrease in size to that of the native structure or are comparable in size to the native state. αTS and DHFR are distinct in this regard owing to the nonmonotonic behavior of their apparent size. Whether this behavior is related to the number of residues in the protein or the existence of stable folding units or is simply reflecting the different phenomena probed is unclear at present.

The double-kinetic approach utilized in this study to measure the compactness of early refolding intermediates complements the SAXS and light-scattering techniques in several advantageous ways. The high sensitivity permits studies to be performed in the micromolar concentration range, a critical factor for investigations of protein fragments and protein folding intermediates, which often have limited solubility. The rapid time scale for the TCSPC experiment (nanoseconds) enables size measurements over refolding times from ∼20 ms to tens of seconds. Additionally, because the rotational correlation time has a cubic dependence on the hydrodynamic radius, time-resolved anisotropy measurements are well-suited to probe small changes in the compactness of proteins. An important caveat in comparisons of size measurements between scattering and fluorescence techniques is that the fluorescence measurements are not strictly population weighted. In the double-kinetic approach, the nanosecond/picosecond time resolution is utilized to selectively enhance the signal associated with ANS bound states, and hence may preferentially yield information on the more highly structured segments of the protein. By contrast, SAXS and light scattering monitor the structure of the entire polypeptide. The time-resolved fluorescence anisotropy signal provides the only current methodology capable of directly measuring the rotational correlation function of these rapidly collapsed states. Thus, time-resolved anisotropy experiments provide a unique (and complementary) perspec-

tive on global structural changes that occur in protein folding reactions.

ACKNOWLEDGMENT

We are grateful to Drs. Michael Otto, Jason Sutin, and Gina Perez for technical assistance and helpful discussions. We also thank Dr. Katherine Bowers for insightful discussions and for sharing unpublished results.

REFERENCES

1. Kim, P. S., and Baldwin, R. L. (1990) *Annu. Rev. Biochem. 59*, 631−660.
2. Matthews, C. R. (1993) *Annu. Rev. Biochem. 62*, 653−683.
3. Raschke, T. M., and Marqusee, S. (1998) *Curr. Opin. Biotechnol. 9*, 80−86.
4. Englander, S. W., and Mayne, L. (1992) *Annu. Rev. Biophys. Biomol. Struct. 21*, 243−265.
5. Jones, B. E., and Matthews, C. R. (1995) *Protein Sci. 4*, 167−177.
6. Sauder, J. M., and Roder, H. (1998) *Folding and Des. 3*, 293−301.
7. Balbach, J., Forge, V., Lau, W. S., van Nuland, N. A., Brew, K., and Dobson, C. M. (1996) *Science 274*, 1161−1163.
8. Plaxco, K. W., and Dobson, C. M. (1996) *Curr. Opin. Struct. Biol. 6*, 630−636.
9. Luchins, J., and Beychok, S. (1978) *Science 199*, 425−426.
10. Ittah, V., and Haas, E. (1995) *Biochemistry 34*, 4493−506.
11. Lillo, M. P., Szpikowska, B. K., Mas, M. T., Sutin, J. D., and Beechem, J. M. (1997) *Biochemistry 36*, 11273−11281.
12. Eliezer, D., Jennings, P. A., Wright, P. E., Doniach, S., Hodgson, K. O., and Tsuruta, H. (1995) *Science 270*, 487−488.
13. Chen, L., Wildegger, G., Kiefhaber, T., Hodgson, K. O., and Doniach, S. (1998) *J. Mol. Biol. 276*, 225−237.
14. Gast, K., Zirwer, D., Muller-Frohne, M., and Damaschun, G. (1998) *Protein Sci. 7*, 2004−2011.
15. Socci, N. D., Onuchic, J. N., and Wolynes, P. G. (1998) *Proteins: Struct., Funct., Genet. 32*, 136−158.
16. Arai, M., Ikura, T., Semisotnov, G. V., Kihara, H., Amemiya, Y., and Kuwajima, K. (1998) *J. Mol. Biol. 275*, 149−162.
17. Panick, G., Malessa, R., Winter, R., Rapp, G., Frye, K. J., and Royer, C. A. (1998) *J. Mol. Biol. 275*, 389−402.
18. Semisotnov, G. V., Kihara, H., Kotova, N. V., Kimura, K., Amemiya, Y., Wakabayashi, K., Serdyuk, I. N., Timchenko, A. A., Chiba, K., Nikaido, K., Ikura, T., and Kuwajima, K. (1996) *J. Mol. Biol. 262*, 559−574.
19. Lakowicz, J. R. (1983) *Principles of fluorescence spectroscopy*, Plenum Press, New York.
20. Jones, B. E., Beechem, J. M., and Matthews, C. R. (1995) *Biochemistry 34*, 1867−1877.
21. Beechem, J. M. (1997) *Methods Enzymol. 278*, 24−49.
22. Jennings, P. A., and Wright, P. E. (1993) *Science 262*, 892−896.
23. Eliezer, D., Chiba, K., Tsuruta, H., Doniach, S., Hodgson, K. O., and Kihara, H. (1993) *Biophys. J. 65*, 912−917.
24. Hyde, C. C., Padlan, S. A., Miles, E. W., and Davies, D. R. (1988) *J. Biol. Chem. 263*, 17857−17871.
25. Matthews, C. R., and Crisanti, M. M. (1981) *Biochemistry 20*, 784−792.
26. Saab-Rincon, G., Gualfetti, P. J., and Matthews, C. R. (1996) *Biochemistry 35*, 1988−1994.
27. Gualfetti, P. J., Bilsel, O., and Matthews, C. R. (1999) *Protein Sci*. (submitted for publication).
28. Bilsel, O., Zitzewitz, J. A., Bowers, K. E., and Matthews, C. R. (1999) *Biochemistry 38*, 1018−1029.
29. Kirschner, K., Wiskocil, R. L., Loehn, M., and Rezeau, L. (1975) *Eur. J. Biochem. 60*, 513−523.
30. Tsuji, T., Chrunyk, B. A., Chen, X., and Matthews, C. R. (1993) *Biochemistry 32*, 5566−5575.
31. Pace, C. N., Shirley, B. A., and Thomson, J. A. (1989) in *Protein structure: A practical approach* (Creighton, T. E., Ed.) pp 311−330, IRL Press, Oxford, England.
32. Tanford, C. (1968) *Adv. Protein Chem. 23*, 122−282.
33. Matthews, C. R. (1987) *Methods Enzymol. 154*, 498−511.
34. Henry, E. R., and Hofrichter, J. (1992) *Methods Enzymol. 210*, 129−192.
35. Marquardt, D. W. (1963) *J. Soc. Ind. Appl. Math. 11*, 431−441.
36. Beechem, J. M. (1992) *Methods Enzymol. 210*, 37−54.
37. Slavik, J. (1982) *Biochim. Biophys. Acta 694*, 1−25.
38. Saab-Rincon, G., Froebe, C. L., and Matthews, C. R. (1993) *Biochemistry 32*, 13981−13990.
39. Kumar, T. K., Jayaraman, G., Lin, W. Y., and Yu, C. (1996) *Biochim. Biophys. Acta 1294*, 103−105.
40. Weast, Robert C., Ed. (1972−1973) *Handbook of Chemistry and Physics*; CRC Press, Cleveland, OH.
41. Beasty, A. M., Hurle, M. R., Manz, J. T., Stackhouse, T., Onuffer, J. J., and Matthews, C. R. (1986) *Biochemistry 25*, 2965−2974.
42. Crisanti, M. M., and Matthews, C. R. (1981) *Biochemistry 20*, 2700−2706.
43. Ptitsyn, O. B. (1995) *Adv. Protein Chem. 47*, 83−229.
44. Chen, X. (1994) Thesis, Department of Chemistry, Pennsylvania State University, University Park, PA.
45. Engelhard, M., and Evans, P. A. (1995) *Protein Sci. 4*, 1553−1562.
46. Miles, E. W., Yutani, K., and Ogasahara, K. (1982) *Biochemistry 21*, 2586−2592.
47. Chen, X., Rambo, R., and Matthews, C. R. (1992) *Biochemistry 31*, 2219−2223.
48. Ogasahara, K., Matsuhita, E., and Yutani, K. (1993) *J. Mol. Biol. 234*, 1197−1206.
49. Garcia de la Torre, J., and Bloomfield, V. (1981) *Q. Rev. Biophys. 14*, 81−139.
50. Garcia de la Torre, J., Navarro, S., Martinez, M. C. L., Diaz, F. G., and Cascales, J. J. L. (1994) *Biophys. J. 67*, 530−531.
51. Venable, R. M., and Pastor, R. W. (1988) *Biopolymers 27*, 1001−1014.
52. Copie, V., Tomita, Y., Akiyama, S. K., Aota, S.-i., Yamada, K. M., Venable, R. M., Pastor, R. W., Krueger, S., and Torchia, D. A. (1998) *J. Mol. Biol. 277*, 663−682.
53. Dunbar, J., Yennawar, H. P., Banerjee, S., Luo, J., and Farber, G. K. (1997) *Protein Sci. 6*, 1727−1733.
54. Tirado-Rives, J., Orozco, M., and Jorgensen, W. L. (1997) *Biochemistry 36*, 7313−7329.
55. Ogasahara, K., and Yutani, K. (1994) *J. Mol. Biol. 236*, 1227−1240.
56. Segel, D. J., Fink, A. L., Hodgson, K. O., and Doniach, S. (1998) *Biochemistry 37*, 12443−12451.
57. Uversky, V. N., Karnoup, A. S., Segel, D. J., Seshadri, S., Doniach, S., and Fink, A. L. (1998) *J. Mol. Biol. 278*, 879−894.
58. Godzik, A., Skolnick, J., and Kolinski, A. (1992) *Proc. Natl. Acad. Sci. U.S.A. 89*, 2629−2633.
59. Saab-Rincon, G. (1994) Thesis, Department of Chemistry, Pennsylvania State University, University Park, PA.
60. Panchenko, A. R., Luthey-Schulten, Z., and Wolynes, P. G. (1996) *Proc. Natl. Acad. Sci. U.S.A. 93*, 2008−2013.
61. Wallqvist, A., Smythers, G. W., and Covell, D. G. (1997) *Protein Sci. 6*, 1627−1642.
62. Gegg, C. V., Bowers, K. E., and Matthews, C. R. (1997) *Protein Sci. 6*, 1885−1892.
63. Zitzewitz, J. A., Gualfetti, P. J., Perkons, I. E., Wasta, S. A., and Matthews, C. R. (1999) *Protein Sci*. (in press).
64. Grantcharova, V. P., Riddle, D. S., Santiago, J. V., and Baker, D. (1998) *Nat. Struct. Biol. 5*, 714−720.
65. Finn, B. E., Chen, X., Jennings, P. A., Saalau-Bethell, S. M., and Matthews, C. R. (1992) in *Protein Engineering: A Practical Approach* (Rees, A. R., Sternberg, M. J. E., and Wetzel, R., Eds.) pp 167−189, IRL Press, Oxford, England.

BI9829433